

# Expansion Mechanism of Vacancy in $\alpha$ -Ti under Tensile Loading

Li Junye<sup>1</sup>, Song Juncheng<sup>1</sup>, Zang Xiang<sup>1</sup>, Zhao Weihong<sup>1</sup>, Zhang Xinming<sup>1</sup>,  
Yan Wenduan<sup>2</sup>

<sup>1</sup>Ministry of Education Key Laboratory for Cross-Scale Micro and Nano Manufacturing, Changchun University of Science and Technology, Changchun 130022, China; <sup>2</sup>College of Photoelectrical and Electromechanical Engineering, Minnan University of Science and Technology, Quanzhou 362000, China

**Abstract:** Using the molecular dynamics method, we applied tensile loads in different directions to a preset-microcracks  $\alpha$ -Ti model. Through the observation of the changes in the pores and dislocations of the  $\alpha$ -Ti model, we revealed the mechanism of the pore growth and the potential energy distribution. We found that under the tensile load along [0001], the perpendicular direction of the close-packed plane, the preset crack in the model closes up, the clusters on both sides occupy the gap of crack defect, showing an obvious necking phenomenon, and part of the hcp lattice transform into the fcc lattice to plane, which derive a variety of dislocations with higher density in the crystal. Therefore, it can bear more press. Under the tensile load along [12 $\bar{3}$ 0], the dislocation types are mainly  $1/3[1\bar{2}10]$  with less total length than in [0001]. The crack grows into a circular cavity. The cavity and sliding band divides the absorption energy regions into four parts. The lattice transformations are mainly from hcp to amorphous structure. The direction of the slip band depends on the material lattice and the position depends on the initial crack. Load on [0001] makes the necking phenomenon of the model prominent, and the crack defect vacancies are occupied by the clusters on left and right sides. Therefore, when loaded on [0001] the  $\alpha$ -Ti has better plasticity and ductility than loaded on [12 $\bar{3}$ 0].

**Key words:**  $\alpha$ -Ti; cavity growth; crystal orientation; dislocation; molecular dynamics

Due to its excellent thermal stability, creep resistance, and low cycle fatigue properties, titanium has become an essential material for the manufacture of aero-engine turbine disks and blades. Because of its adaptability to various extreme working environment, it can be applied to load-bearing members subjected to cyclic loading<sup>[1]</sup>. The most common form of titanium,  $\alpha$ -Ti, has features of low symmetry, few slip systems, and prominent anisotropy, which make the influence of lattice orientation on  $\alpha$ -Ti-based materials a research focus<sup>[2]</sup>.

The fatigue life of titanium and its alloys is very sensitive to the surface and subsurface state of the material. The main factor determining metal part's fatigue life is the fatigue cracks nucleation. In the molding process and heat treatment process, metal parts inevitably have internal defects, such as impurity pores and uneven lattice. For components with poor surface conditions, the crack initiation accelerates a lot. Small holes or cracks may have the possibility of expanding into macroscopic holes, which cause dangers. Besides, in the processes of surface removal,

Received date: January 05, 2020

Foundation item: National Natural Science Foundation of China (51206011, U1937201); Science and Technology Development Program of Jilin Province (20170204064GX); Project of Education Department of Jilin Province (JJKH20190541KJ); Science and Technology Program of Changchun City (18DY017)

Corresponding author: Zhang Xinming, Ph. D., Professor, College of Mechanical and Electrical Engineering, Changchun University of Science and Technology, Changchun 130022, P. R. China, E-mail: zxm@cust.edu.cn

Copyright © 2021, Northwest Institute for Nonferrous Metal Research. Published by Science Press. All rights reserved.

the integrity of the surface is hard to guarantee. Reduced roughness, surface damage, and surface residual stress can damage the surface condition of the material<sup>[3]</sup>.

Since the details of cracks are difficult to detect, especially in the experiment process, it is complex to study the microcrack transmission through experimental methods<sup>[4]</sup>. Likewise, the finite element analysis method has inherent disadvantages: the crack propagation in the simulation process often cannot pass through the model, so the grid cells do not accurately reflect the behavior of materials at the nanoscale. Based on Newton's mechanical equations, the molecular dynamics research on the atomic motions can extract samples from a large number of particles, and then calculate atomically and integrally to obtain the macroscopic properties of the system.

Verkhovtsev et al. observed how different indenter types can affect the indentation result of the titanium monocrystal<sup>[5]</sup>. Rawat and Mitra et al. located continuous stress on monocrystalline titanium in molecular dynamics simulation. They detected a lot of twinings and dislocations in the investigation<sup>[6]</sup>. Frolov T, Olimsted D L, and their team studied the grain boundary position of the dense hexagonal lattice metal through molecular dynamics simulation. The hindrance of the crack on another linear defect proves that the dislocation can passivate the crack tip<sup>[7]</sup>. Feng et al.<sup>[8]</sup> used the simulation and found that the larger the microcrack inclination angle is, the faster the crack growth rate becomes. Xiangguo Zeng et al.<sup>[9]</sup> combined the Monte Carlo method in molecular dynamics with finite element analysis to predict the fracture toughness and crack propagation of titanium alloys. Kolobov et al.<sup>[10]</sup> simulated the high-speed deformation of  $\alpha$ -Ti at a pressure of 20 GPa and a temperature of 700 K, and established a plastic deformation mechanism including sliding along the prism surface and  $\alpha$ - $\omega$  transition. Doyle and Barrett et al.<sup>[11]</sup> used the MD method to model the phase transition of titanium and verified the correctness of MEAM potential by the transition temperature prediction.

Current scholars are still puzzled at how necking phenomenon influence the evolution of defects. The researches on the energy absorption and distribution of the cavity growing process are still insufficient. In this paper, we use the molecular dynamics method to analyze the partitioning law of pores and slip zones on the energy absorption region of the model system. The tensile load in different directions is applied to the  $\alpha$ -Ti model with preset microcracks. We observe the growth of the crack in the model and the emission, motion, and plugging of the dislocations, and reveal the mechanism of the crack growth.

## 1 Simulation Model Establishment

### 1.1 Selection of the basic model and potential function

At normal pressure and temperature, the titanium is in the form of  $\alpha$ -Ti, a hexagonal close-packed structure (hcp). The  $\alpha$ -Ti's lattice constant is  $a=0.295$  nm,  $c/a=1.59$ . Titanium is converted to  $\beta$ -Ti, in a body-centered cubic structure (bcc) when it is above 882.5 °C but below the melting point.

In the simulation box, the crystal orientations  $[10\bar{1}0]$ ,  $[0001]$ , and  $[12\bar{3}0]$  are the axes of  $x$ ,  $y$ , and  $z$ , respectively. The simulation area is shown in Fig.1. The model size is  $50 \times 3 \times 4$  lattice units.

The blue region in Fig.1 is the upper boundary layer, the dark yellow is the lower boundary layer, and the middle part is the Newtonian layer. The boundary layer is used to maintain the integrity of the system, control the transfer of load and heat, and the Newtonian layer is the central area of crack growth.

The elongated microcracks of  $8 \times 0.2 \times 0.2$  lattice units are preset at the center of the model by removing atoms in the specified area.

Fig.2 is the cutaway view of the  $XOY$  plane with a thickness of 0.2 nm. After presetting the microcrack, we use the Andersen Thermostat method for 10 000 steps at the fixed temperature. After the relaxation process, the atom reaches the equilibrium position and only maintains the thermal motion. We use the cladding type as the boundary condition on the tensile direction, and use the periodic boundary conditions on the other two directions. The boundary layer is applied loads in different orientations in the NVE micro-regular ensemble. The data of the atomic position information, atomic potential energy, its force distribution, the total energy of the system, and other essential parameters is output, and then is imported into the visualization software for analysis.

We adopt EAM (embedded atomic potential function) as the potential function. EAM is a multi-body potential, which takes the charge field formed by the electron array around the nucleus into account. The expression of the

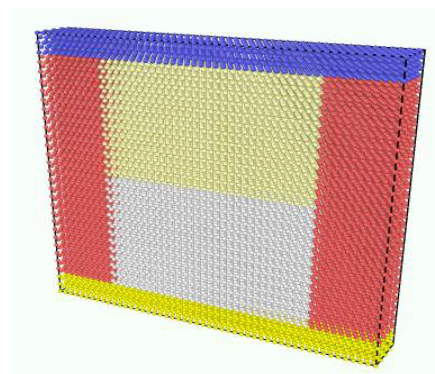


Fig.1 Model diagram

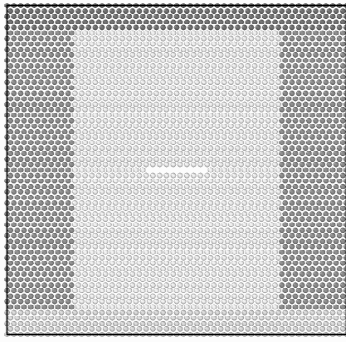


Fig.2 XOY plane slice

EAM potential function is shown in formula (1):

$$E_i = F_\alpha \left( \sum_{j \neq i} \rho \beta(r_{ij}) \right) + \frac{1}{2} \sum_{j \neq i} \phi \alpha \beta(r_{ij}) \quad (1)$$

Where  $E_i$  is the energy of the  $i$  atom;  $F$  is the embedding energy, a function of the atomic electron density  $\rho$ ;  $\phi$  is the atom-to-potential interaction;  $\alpha$  and  $\beta$  represent the type of atom  $i$  and atom  $j$ , respectively. In the function, the  $F$  is a crucial term to characterize the EAM potential function as a multi-body potential function. The atom  $j$  is all the neighboring atoms within the intercept radius of the atom  $i$ .

## 1.2 Placing and loading method

As a hexagonal lattice, the crystal plane and crystal orientation are always described in four axes. The three axes in the Cartesian coordinate system are shown in Fig.3.

The ideal close-packed hexagonal lattice has only one slip plane,  $\{0001\}$ , which is also a close-packed lattice surface, with three slip systems. However, the axial ratio of  $\alpha$ -Ti,  $c/a$ , is lower than the ideal  $c/a$  of the hcp lattice, 1.633, which makes  $\{0001\}$  of  $\alpha$ -Ti no longer a close-packed plane. The slip plane transfer to the cylinder plane,  $\{10\bar{1}0\}$ , and the tilted plane,  $\{10\bar{1}1\}$ , as shown in Fig.4. Thus,  $\alpha$ -Ti lattice has six slip planes, two slip directions, and a total of 12 slip systems.

The cylinder plane,  $\{10\bar{1}0\}$ , has three centrosymmetric orientations, while the tilted plane,  $\{10\bar{1}1\}$ , has six of them. Due to the lack of lattice slip systems in  $\alpha$ -Ti, the lattice structure has poor deformability adjustment, which makes more initiations of dislocation nucleus and phase transition<sup>[12,13]</sup>. It is effortless to induce twin formation when the lattice of the hexagonal structure is densely packed. That is because the slip systems that can be arranged to adjust deformation is relatively weak. The difference between the twin formation process and the slip process is that the twin nucleation requires higher stress. Thus, when the energy absorption from the deformation is slower, twins are more likely to be applied as the deformation pattern<sup>[14,15]</sup>.

After slipping, most metals have twin nucleus in the

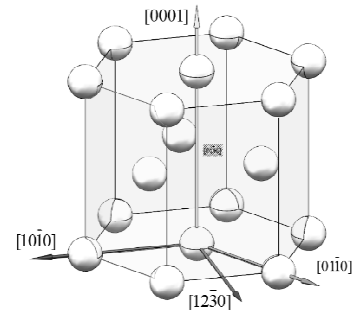
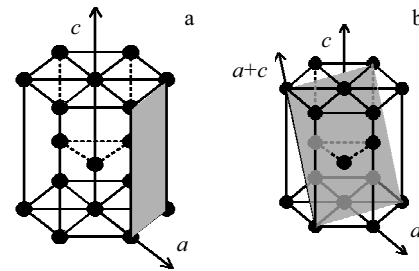


Fig.3 Hexagonal close-packed lattice and its crystal orientations

Fig.4 Cylindrical slip and the oblique-slip of  $\alpha$ -Ti: (a) the  $\{10\bar{1}0\}$  plane and (b) the  $\{10\bar{1}1\}$  plane

position of the peak stress area at the dislocation clusters. Since the stress required for the transmission of twins is much lower than the necessary stress to nucleate it, once twin formed, the shear stress is higher than the critical value of twin motion, and the twins undergo motional growth<sup>[16]</sup>. When the densely packed hexagonal structural material is deformed, a large amount of slip occurs first, and the dislocations are congested somewhere to form twins. At this point, the high stress in this region immediately triggers twin transmissions.

The dense hexagon has a high asymmetry which can be quantitatively estimated when it is compared with other common cubic crystal structures, e.g., face center cube, body center cube, and diamond cubic structure. When the generalized Hooke's law completely describes the linear elastic deformation of the crystal material, 36 elastic constants of the material are required in the form. These 36 constants are not linearly independent. The symmetry of the atomic spatial arrangement of the crystal results in its truly far less independent elastic constants: the symmetry of the triclinic system has the most independent elastic constants, twenty-one; the cubic lattice is the most symmetrical—it has only three independent elastic constants. There are five constants in hexagonal lattices, so its anisotropy still needs attention.

Overall, the influence of the load direction is a focus on the mechanical behavior study of the crack growth. In this

paper we change the orientation of loading. We put the crystal orientation of  $\{0001\}$ , and observe the cavity growth under the stress of  $[12\bar{3}0]$  and  $[0001]$ . As shown in Table 1 The crystal orientation is shown in Fig. 3, and the tensile load is kept at 0.05 nm/ps.

## 2 Result of Simulation and Its Analysis

### 2.1 Cavity growth analysis

Fig.5 and Fig.6 show the crack growth after stretching in  $[0001]$  and  $[12\bar{3}0]$ . In the simulation of  $[0001]$  stretch, the strain of the model increases in the late stage of simulation. Although there is an evident necking phenomenon, the crack becomes much smaller during the necking process. Besides, it's worth noting that there's no interaction acting between the atoms around the crack, so no atomic bond is regenerated, which means the defect is not fixed, only occupied by the cluster close to the neck.

In the simulation of  $[12\bar{3}0]$  stretch, the crack evolves into a circular void and expands in both the stretching direction and its vertical orientation. As the crack grows, part of the atoms inside the model migrates to the inner surface of the cavity.

The  $\alpha$ -Ti shows better ductility under stretch in  $[0001]$  than in  $[12\bar{3}0]$ . Although the overall plasticity of hcp lattice is reduced due to poor lattice transmission ability, the plasticity in the  $[0001]$  direction is the best. The  $\alpha$ -Ti can be necked without breaking.

### 2.2 Internal stress analysis

With the expansion of the atomic displacement and the distance between atoms, the potential energy increases until the original lattice crashes. The interactions and constraints among the atoms either decrease or disappear. As the potential of the lattice system accumulates, the atoms in the lattice are activated, strengthening the motion, breaking the lattice structure. The atoms become chaotic and rearranged to present vacancies. An amorphous structure grows at the crack tip, which makes the crack unstable and expand.

Fig.7 is a distribution diagram of the atomic force in the tensile direction in three different stages. Before the load is applied, the atomic force is evenly distributed. After the load is applied, the shape of the model abruptly changes at the crack tip, and significant stress concentration occurs. The atoms at the crack tip are stress-activated and disordered. Thus they are gradually deviating from the original position in the lattice.

**Table 1** Crystal orientations corresponding to coordinate axes

Stretching directions	$[12\bar{3}0]$	$[0001]$
X axis	$[10\bar{1}0]$	$[12\bar{3}0]$
Y Axis	$[12\bar{3}0]$	$[10\bar{1}0]$
Z Axis	$[0001]$	$[0001]$
Atoms account	48865	48980

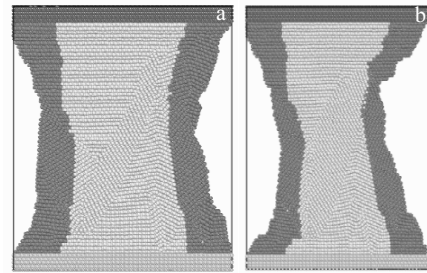


Fig.5 Cavity growth with traction along  $[0001]$ : (a) middle stage and (b) late stage

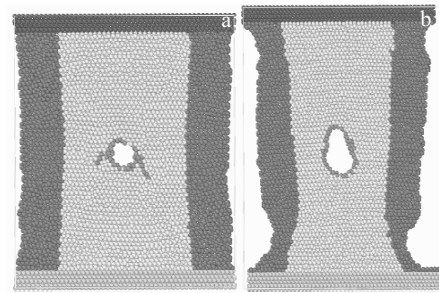


Fig.6 Cavity growth with traction along  $[12\bar{3}0]$ : (a) middle stage and (b) late stage

Along with the load being applied, the force distribution begins to be chaotic. As shown in Fig.7, the green area is where the stress is the even, the red is the higher, and the green is lower. It's evident that the stress in the cutaway plane is fluctuating. The stress transmits and stacks near the dislocation and crack, activates dislocation nucleation, and proliferates and moves through the slip system to almost the whole Newtonian layer. The dislocations that slip and stack on the dislocation bands make the stress distribution more complicated. The plug part of  $\alpha$ -Ti is with the highest stress. In the subsequent simulations, the crack defects continue to deform. The crack expands in the vertical direction as the model strain increases and grows into a circular cavity.

The nucleus of the dislocations at the crack tip and the derivation of twins hinder the crack to continue its expansion. As the cavity grows, the crack tip eventually becomes blunt. Then, no longer has a sharp shape-shifting that may cause stress concentration: the stress redistribution is relatively uniform. In the late stage, the atomic force distribution of the whole system becomes disordered.

### 2.3 Lattice transformation analysis

In the Akland bond angle analysis, as shown in Fig.8, the red atoms are atoms of hcp structures. When stretched by an external load in  $[0001]$ , part of the hcp lattice undergoes a phase transition to the fcc lattice structure (the green atoms); and stretching in other directions causes hcp lattice to turn to a messy amorphous structure (white atoms). Since the

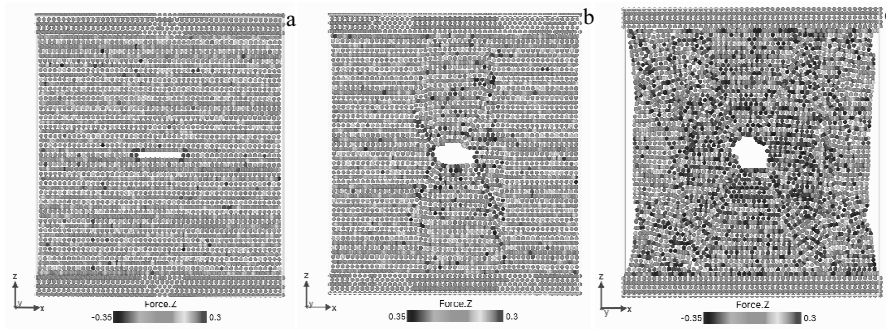


Fig.7 Diagram of atomic force in tensile direction (10 eV/nm): (a) 2000 steps, (b) 10000 steps, (c) 40000 steps

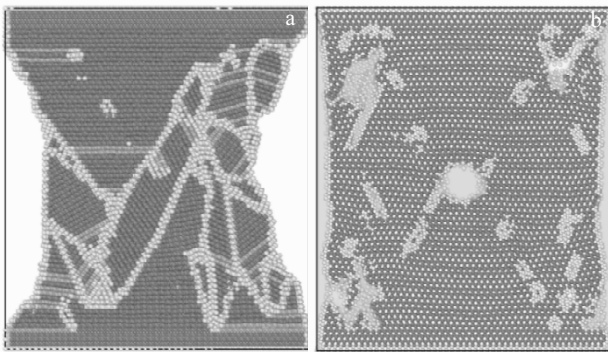


Fig.8 Lattice type and quantity, dislocation type and length: (a) traction in  $[0001]$  and (b) traction in  $[12\bar{3}0]$

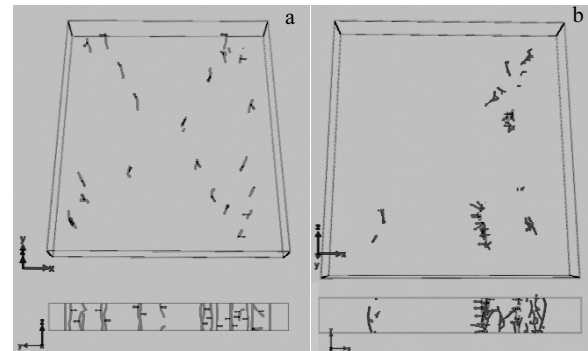


Fig.9 Dislocation lines and Burgers vector graph: (a) traction in  $[12\bar{3}0]$  and (b) traction in  $[0001]$

lattice change in the  $[0001]$  direction can store considerable energy, the  $\alpha$ -Ti presents greater plasticity than other directions. Moreover, under the load in  $[0001]$ , the phase-transition into fcc remains crystal structure. Lattice can extend over a stretch distance while maintaining atoms bond and leaving a deposit in atomic scattering brittle cleavage crack tip less likely to occur.

Fig.9 is graph of dislocation lines and Burgers vector. The type of dislocation produced by the  $[12\bar{3}0]$  stretch is relatively simple, with only 22 segments of  $1/3[1\bar{2}10]$  type, with a total length of 19.38 nm. Under the stretch of  $[0001]$ , the  $\alpha$ -Ti has a variety of dislocations with a total length of 26 nm, which includes Perfect dislocation, Shockley dislocation, and Stair-rod dislocation. The length of the dislocation line is directly related to the amount of strain energy in the crystal. The total strain energy per unit length dislocation is as shown in Eq.(2):

$$W = \alpha G b^2 \quad (2)$$

Where  $\alpha$  denotes a parameter determined by the density and type of dislocations, which usually takes ranges from 0.5 to 1.0;  $b$  is the Burgers vector, which is used to describe the slip distance, and  $G$  is the shear modulus.

The position of the crack tip determines where the atomic dislocation is. The dislocation nucleus is emitted along the

slip direction—each pair of dislocations intersects near the end of the crack and expands symmetrically. As the stretch continues, dislocations are expanding on this plane. The system stores the external energy as potential.

#### 2.4 Energy analysis

Fig.10 shows the atomic potential energy map. The higher potential region in Fig.10 includes the inner edge of the cavity and the periphery of the dislocation. The energy dissipation is mainly caused by the cavity growth, the dislocation emission, and movement accompanying the elongation or fracture of the atomic bond. We regard the defect-containing  $\alpha$ -Ti as a steady-state force field superimposed by two stress systems: one is the force field generated by the applied load, and the other is the stress field of the inner defect group. When the increasing external load breaks the balance, the system absorbs energy through atomic bond rupture, and transmits stress through dislocations to forms a new force field until the equilibrium recovers.

At the initial stage of the simulation, the atomic potential energy at the slip area is higher than in other regions. Therefore, the atoms around the slip area are activated first. In the subsequent stage, the potential energy distribution is divided into four districts in the form of  $X$ : the left and

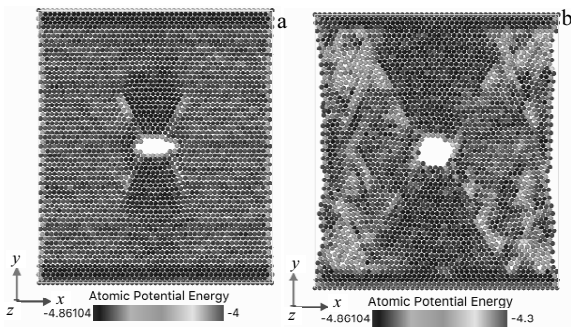


Fig.10 Atomic potential energy distribution (eV): (a) traction in  $[12\bar{3}0]$  and (b) traction in  $[0001]$

right are the stretched regions, with some lattice vacancy presenting, the atomic spacing increases, as well as the potential energy; the upper and lower regions become denser because of the material necking, potential energy has not changed significantly. Compared with Fig.8b, the lattice in upper and lower areas have not significantly changed. The atom bonds are well-preserved. Thus, no obvious change presents in potential energy map on these areas.

The common effect caused by both the cavity and the slip belt divides the potential energy distribution area. As described above, the position of the slip belt is fixed by the initial crack tip position and the material lattice geometry. Therefore, under the premise of determining the material and the stretching direction, the initial crack position determines where the material mainly absorbs energy.

In order to verify this theory, we widen the length of the  $\alpha$ -Ti model and do the  $[12\bar{3}0]$  stretch once more.

In Fig.11, the potential energy map is still divided into four areas. Compared with Fig.10, the sloping angles of the dividing lines are basically the same. The left and right areas are the main changing stage of potential energy. The only difference between the widened model and origin is the distribution of the potential energy is "diluted" in the left and right areas, so the map of the widened model is "darker" than the original. The theory has been verified.

In Fig. 12, the trend of potential energy is the same as the total energy trend. The difference between the total energy and the potential energy is the total kinetic energy. The simulated ambient temperature is kept constant, so the kinetic energy transfers between the outer Newtonian layer and the inner Newtonian layer. Thus, the sum of the atomic kinetic energy is unchanged, but only a small fluctuation occurs. Therefore, the total energy change in value is approximately the potential energy change in value. When the stretch is working on the model, it mainly stores energy as potential. From Fig. 10, there are dislocations or holes in the light blue region with higher potential energy. These areas with higher energy are adjacent to the dislocation or

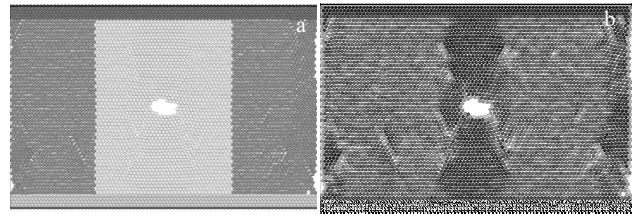


Fig.11 Atomic potential energy map of the widened model: (a) atom position in the widened model and (b) potential energy distribution in the widened model

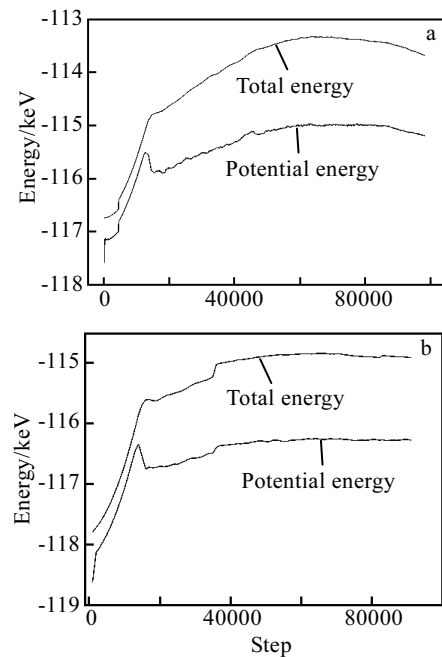


Fig.12 System energy and potential energy curves: (a) traction in  $[12\bar{3}0]$  and (b) traction in  $[0001]$

the cavity. In other words, the generation of the crack and the emission of the dislocation is stimulated by the external loads. Dislocations and cavity are competitively generated to become the main force to eliminate the effects of external loads.

The total energy curve of the tensile potential energy in the  $[0001]$  direction is higher than the curve stretched in  $[12\bar{3}0]$  direction, in which the crystal lattice has a higher energy threshold in this direction, and more energy leads to more phase transitions in the lattice, which make the dislocations longer and more. At the later stage of the simulation, the lattice deformability is still not fully exerted. In the late stage, the external load does not cause atomic bond failure phenomena as much as the experiment in  $[12\bar{3}0]$ , and the energy curve does not show a significant downward trend. With the external load on the model, the lattice can absorb much more energy in the form of the phase transitions and dislocations. As a result affected by the two

factors, the system has a drop in energy so that the curve will fluctuate slightly. The load in the  $[12\bar{3}0]$  direction in the later stage leads to a large amount of deformability and saturated lattice damage.

### 3 Conclusions

1) When the microcrack-preset  $\alpha$ -Ti model is under stretching load in  $[0001]$ , part of the HCP lattice undergoes a phase transition to the bcc structure, with many types of dislocations, high density, and considerable absorption of energy. In the meantime, obvious necking occurs in the stretching direction, and the clusters move toward the center on both sides of the cavity; the stretching in the  $[12\bar{3}0]$  direction is more likely to change the hcp lattice to the amorphous structure. The necking of the model is not prominent, resulting in stress concentration at the tip of the crack, which in turn evolves into a circular cavity.

2) Before the initial crack is unstable, stress concentration presents near the tip. Energy dissipation mainly occurs through the growth of the crack with atomic bonds and the emission and movement of dislocations. In the later period, a large number of atomic bonds are broken to absorb the energy. The  $[12\bar{3}0]$  tensile total energy curve shows a decrease. As for the model loaded in  $[0001]$ , the lattice absorbs energy more strongly, and the energy curve does not decline.

3) Having the cavity formed, the direction of the slip plane is regular and clear. The four slip belts are axisymmetric concerning the horizontal and vertical directions, intersecting at the left and right crack tips. The upper and lower regions blocked by the cavity have little energy changes, and the left and right regions serve as the primary energy buffer. The relative position of the energy-unchanged area won't change, and the only difference it will have is the local potential energy concentration in the left and right area.

### References

- 1 Ezugwu E O, Wang Z M. *Journal of Materials Processing Technology* [J], 1997, 68(3): 262
- 2 Pervaiz S, Rashid A, Deiab I et al. *Materials and Manufacturing Processes*[J], 2014, 29(3): 219
- 3 Fu L B, Yang X H, Dong P S et al. *Applied Mechanics and Materials*[J], 2011, 66-68: 838
- 4 Pitt F, Abhyankar S, Labossiere P et al. *Journal of Materials Engineering and Performance*[J], 2007, 16(2): 155
- 5 Verkhovtsev A V, Yakubovich A V, Sushko G B et al. *Computational Materials Science*[J], 2013, 76: 20
- 6 Rawat Sunil, Mitra Nilanjan. *Computational Materials Science*[J], 2018, 141: 19
- 7 Frolov T, Olimsted D L, Asta M et al. *Nature Communications*[J], 2013(4): 1899
- 8 Feng R C, Lu J T, Li H Y et al. *Strength of Materials*[J], 2017, 49: 75
- 9 Zeng Xiangguo, Han Tixin, Guo Yang et al. *Engineering Fracture Mechanics*[J], 2018, 190: 120
- 10 Kolobov Y R, Lipnitskii A G, Ivanov M B et al. *Russian Physics Journal*[J], 2012, 54(8): 918
- 11 Doyle D, Barrett C D, Carino R L et al. *Modelling and Simulation in Materials Science and Engineering*[J], 2018, 26(6): 1361
- 12 Fung K, Tang C, Cheung C et al. *Key Engineering Materials* [J], 2014, 626(6): 5
- 13 Pond R C, Serra A, Bacon D J. *Acta Materialia*[J], 1999 (5): 15
- 14 Swygenhoven H Van, Caro A, Farkas D. *Materials Science & Engineering A*[J], 2001: 309-310: 440
- 15 Hong D H, Lee T W, Lim S H et al. *Scripta Materialia* [J], 2013(5): 33
- 16 Li D, Meng F Y, Ma X Q et al. *Material Science & Technology*[J], 2011, 27(11): 1025

## 拉伸载荷下 $\alpha$ -Ti 孔洞生长的机制研究

李俊焯<sup>1</sup>, 宋俊成<sup>1</sup>, 臧翔<sup>1</sup>, 赵伟宏<sup>1</sup>, 张心明<sup>1</sup>, 颜文段<sup>2</sup>

(1. 长春理工大学 跨尺度微纳制造教育部重点实验室, 吉林 长春 130022)

(2. 闽南理工学院 光电与机电工程学院, 福建 泉州 362000)

**摘要:** 利用分子动力学方法, 对含有预置微裂纹  $\alpha$ -Ti 模型施加不同方向拉伸载荷, 通过观察模型内孔洞及位错的变化情况, 揭示了孔洞生长的机制与初始缺陷对材料吸收能量在不同划分区域的规律。研究发现: 当拉伸载荷沿着垂直于密排面的 $[0001]$ 方向时, 预置裂纹愈合,  $\alpha$ -Ti 会从 hcp 晶格转换为 fcc 晶格, 从而使晶体中的位错种类更多、密度更大、能量吸收率更高; 当拉伸载荷沿着  $[12\bar{3}0]$  方向拉伸时, 位错种类主要为  $1/3[1\bar{2}10]$  类型, 裂纹则生长为一定尺寸的孔洞, 孔洞与滑移带对模型体系吸收能量区域有划分作用, 转换的晶格主要为非晶结构, 滑移带方向取决于材料晶格, 位置取决于初始裂纹;  $\alpha$ -Ti 沿 $[0001]$ 晶向拉伸后模型明显颈缩, 裂纹缺陷空位被两侧团簇占据,  $\alpha$ -Ti 沿 $[0001]$ 晶向拉伸比沿  $[12\bar{3}0]$  方向拉伸时拥有更好的塑性和延展性。

**关键词:**  $\alpha$ -Ti; 孔洞生长; 晶体取向; 位错; 分子动力学

作者简介: 李俊焯, 男, 1981年生, 博士, 教授, 长春理工大学机电工程学院, 吉林 长春 130022, E-mail: fstvng@163.com